PHYSICAL REVIEW A **93**, 041802(R) (2016)

# Observation and characterization of cavity Rydberg polaritons

Jia Ningyuan, Alexandros Georgakopoulos, Albert Ryou, Nathan Schine, Ariel Sommer, and Jonathan Simon
*Department of Physics and James Franck Institute, University of Chicago, Chicago, Illinois 60637, USA*
(Received 5 November 2015; published 13 April 2016)

We experimentally demonstrate the emergence of a robust quasiparticle, the cavity Rydberg polariton, when an optical cavity photon hybridizes with a collective Rydberg excitation of a laser-cooled atomic ensemble. Free-space Rydberg polaritons have recently drawn intense interest as tools for quantum information processing and few-body quantum science. Here, we explore the properties of their cavity counterparts in the single-particle sector, observing an enhanced lifetime and slowed dynamics characteristic of cavity dark polaritons. We measure the range of cavity frequencies over which the polaritons persist, corresponding to the spectral width available for polariton quantum dynamics, and the speed limit for quantum information processing. Further, we observe a cavity-induced suppression of inhomogeneous broadening channels and demonstrate the formation of Rydberg polaritons in a multimode cavity. In conjunction with recent demonstrations of Rydberg-induced cavity nonlinearities, our results point the way towards using cavity Rydberg polaritons as a platform for creating high-fidelity photonic quantum materials and, more broadly, indicate that cavity dark polaritons offer enhanced stability and control uniquely suited to optical quantum information processing applications beyond the Rydberg paradigm.

DOI: 10.1103/PhysRevA.93.041802

Engineered quasiparticles are a powerful tool for many-body physics and quantum information science, providing the opportunity to build particles imbued with properties chosen from multiple constituent systems. Photonic quasiparticles are particularly appealing, as optical structures can control their propagation, and they can be read out and transmitted over long distances. Examples include exciton polaritons in semiconductor microcavities [1–3], whose mass and trapping arise from a photonic component, and mean-field interactions from an excitonic component; magnon polaritons [4–6], providing long-lived storage of quantum information in a collective atomic hyperfine excitation; and surface plasmon polaritons [7], where the photonic component provides tight confinement, and thus strong interactions due to hybridization with a single emitter.

The Rydberg polariton [8–19] has recently emerged as a particularly interesting photonic quasiparticle for nonlinear quantum optics; its Rydberg component provides interactions that are strong at the single-quantum level, enabling single-photon transistors for quantum information processing [20–22], while its photonic component allows interfacing to quantum communication channels [23]. While these particles have been primarily studied in free space, trapping the photonic component in an optical resonator enhances interactions between polaritons [14,24], and promises exquisite control of polariton dispersion [25] necessary to induce photonic BECs [1,26], emergent crystallinity [27–31], and topological fluids in synthetic magnetic fields [27,32–36].

In this Rapid Communication, we observe the cavity Rydberg polariton and characterize its single-body properties, many of which apply to all cavity dark polaritons. We first explore the dark-polariton spectrum, quantitatively demonstrating compression [37,38] compared to the bare cavity spectrum near electromagnetically induced transparency (EIT) resonance, corresponding to a slowdown of dynamics. We investigate the available bandwidth for many-body physics or quantum information processing (QIP) set by the width of the EIT resonance versus the cavity frequency, and demonstrate the connection to the free-space EIT linewidth. We then observe a suppression of inhomogeneous broadening channels and provide a quantitative model for this effect. Finally, we explore dark-polariton physics in a multimode regime with an eye towards few-particle quantum material and QIP experiments.

Our system consists of an ensemble of ground-state atoms in the waist of an optical cavity, as illustrated in Fig. 1(a). A cavity photon ($|c\rangle$) may be absorbed by the atomic ensemble, generating a collective excitation $|e_c\rangle$ of the $|e\rangle$ level, with collective vacuum Rabi frequency $G$. A control laser transfers the $|e_c\rangle$ state to a collective excitation $|r_c\rangle$ of the Rydberg level $|r\rangle$ with Rabi frequency $\Omega$. The eigenstates of the coupled atom-cavity system include a dark state $|D\rangle$ and two bright states $|B\pm\rangle$. When the cavity is tuned to the EIT resonance condition $\delta_c = \delta_R$, with $\delta_c$ the frequency of the cavity mode minus the atomic transition frequency and $\delta_R$ the transition frequency from $|e\rangle$ to $|r\rangle$ minus the frequency of the control laser, the dark state is $|D\rangle = \cos\theta|c\rangle - \sin\theta|r_c\rangle$, where $\theta \equiv \tan^{-1}(G/\Omega)$ is the dark-state rotation angle [9,39]. We study the dark-polariton energy $\hbar\delta_D$ (relative to the atomic resonance) and inverse lifetime $\gamma_D$ by observing the transmission spectrum in cavity Rydberg EIT.

Experiments begin with a laser-cooled $^{87}$Rb atomic sample that we optically transport into the waist of a running-wave bow-tie optical cavity. The cavity is tuned near the atomic $D_2$ transition (780 nm) from the $|g\rangle = 5S_{1/2}(F = 2)$ ground state to the $|e\rangle = 5P_{3/2}(F = 3)$ excited state. The control laser (wavelength 480 nm, waist 29 $\mu$m) that couples to the $|r\rangle = nS_{1/2}$ Rydberg level counterpropagates through the sample. Here, we use primarily $n = 40$. At 780 nm, the cavity has a $\mathrm{TEM}_{00}$ mode waist of 12 $\mu$m $\times$ 11 $\mu$m ($1/e^2$ intensity radii) between the lower mirrors, and a finesse of 2500 [1.8 MHz full width at half maximum (FWHM) linewidth]. We obtain transmission spectra by sweeping the detuning $\delta_L$ of a probe laser (laser frequency minus the atomic transition frequency) linearly over 1 ms and detecting the transmitted light with a single-photon counter. By using sufficiently low principle

 

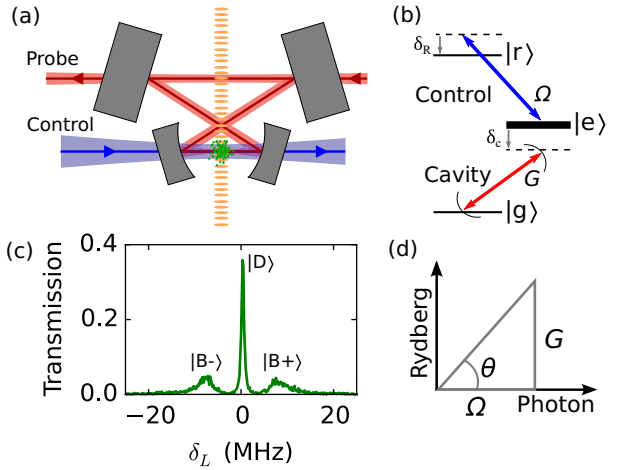


FIG. 1. Cavity Rydberg EIT. (a) Schematic of the experimental setup, showing the $^{87}$Rb atomic sample in the waist of a running-wave cavity after being transported by a moving optical lattice. The cavity mirrors are high finesse at the probe wavelength (780 nm), and antireflection (AR) coated for the control laser (480 nm) that counterpropagates through the sample. (b) Level diagram showing that the cavity mode couples the atomic ground state to an excited state, with collective vacuum Rabi frequency $G$ and detuning $\delta_c$, while the control laser couples the excited state to a Rydberg level, with Rabi frequency $\Omega$ and detuning $\delta_R$. (c) Transmission spectrum as a fraction of the peak empty-cavity transmission showing peaks due to the cavity Rydberg dark polariton state $|D\rangle$ and two bright polariton states $|B\pm\rangle$. Here, $G = 13$ MHz, $\Omega = 7$ MHz, $\delta_c = \delta_R = 0$. (d) Decomposition of the dark polariton into cavity photon and Rydberg components, set by the couplings $G$ and $\Omega$ that define the dark-state rotation angle $\theta$.

quantum numbers and photon densities, we work in a regime of small polariton-polariton interactions and isolate the properties of individual polaritons.

Because the polariton spends much of its time as a collective Rydberg excitation rather than a resonator photon, polariton dynamics are expected to be proportionally slower than those of their photonic constituent [37,38]. We explore this effect in Figs. 2(a)–2(c), where we measure the resonator spectrum as a function of cavity frequency [within each frame of Fig. 2(a)], for several dark-state rotation angles [different frames of Fig. 2(a)]. The energy of the dark polariton tunes more slowly than the cavity itself by a factor set by the dark-state rotation angle, as shown in Fig. 2(c), in quantitative agreement with the first-order expansion [37,40] $\delta_D \approx \delta_c \cos^2\theta + \delta_R \sin^2\theta$.

The utility of polaritons depends on their lifetime: Strong single-photon nonlinearities require an interaction energy [27] greater than the width of the polariton resonance, and photonic materials require stable polaritons to allow well-resolved many-body states [34]. The primary loss channels for dark polaritons are an outcoupling of their photonic component through the cavity and decay of the Rydberg excitation, giving $\gamma_D \approx \kappa \cos^2\theta + \gamma_R \sin^2\theta$ at EIT resonance [37,40]. The right axis in Fig. 2(c) shows $\gamma_D$ obtained from the full width at half maximum of a Lorentzian fit to the dark-polariton peak with the cavity at EIT resonance, compared to theory; it reaches a minimum of 0.26(1) MHz, significantly less than the bare cavity linewidth of 1.8 MHz.

Polariton interactions, as well as spatial dynamics in multimode cavities, would lead to a detuning from EIT resonance. This detuning introduces a fundamental loss channel that has not been explored in previous experimental studies of (ground-state) cavity EIT [38,41–45]. Figure 2(d) shows the dependence of the polariton linewidth on detuning from EIT resonance, in quantitative agreement with a simple model [37,40],

$$\gamma_D \approx \kappa \cos^2\theta + \gamma_R \sin^2\theta + a(\delta_c - \delta_R)^2, \tag{1}$$

with $a \equiv 4\Omega^2 G^2 \Gamma/(\Omega^2 + G^2)^3$ giving the strength of the quadratic term. The cavity detuning required to double the polariton decay rate is $\delta_c - \delta_R = \Delta \equiv \frac{1}{2}\frac{\Omega^2/\Gamma}{\sqrt{\mathrm{OD}}}/\cos^2\theta$ for $\gamma_R \ll \kappa$, where $\mathrm{OD} \equiv \frac{G^2}{\kappa\Gamma}$ is the cavity-enhanced optical depth. When the cavity is detuned by $\Delta$, the dark-polariton energy moves only by $\Delta\cos^2\theta = \frac{1}{2}\frac{\Omega^2/\Gamma}{\sqrt{\mathrm{OD}}}$, which is identical to the free-space EIT linewidth [39].

The cavity EIT bandwidth is also observable in the height (maximum transmission) of the dark-polariton resonance. We explore this behavior in Fig. 2(e), and observe that the peak transmission follows a squared Lorentzian [40],

$$T_D \propto [1 + (\delta_c - \delta_R)^2/(\Gamma_w/2)^2]^{-2}, \tag{2}$$

with $\Gamma_w \approx 2\Delta$ as defined above. The cavity EIT width $\Gamma_w$ determines the bandwidth available for polariton dynamics and interactions. In a multimode cavity, $\Gamma_w$ sets the maximum polariton kinetic energy transverse to the cavity. In a quantum gate based on detuning from EIT resonance [8], the maximum detuning sets a limit on the gate time of $\sim 1/\Gamma_w$.

Compared to ground-state cavity polaritons, Rydberg cavity polaritons exhibit an enhanced sensitivity to inhomogeneous broadening of the collective atomic excitation arising from the Doppler effect (due to the wavelength mismatch in the ladder configuration) and inhomogeneous electric fields (due to the large polarizability of Rydberg atoms). The latter is particularly significant near surfaces [46–48], such as the dielectric mirrors of an optical cavity.

Because these decoherence channels enter the polariton linewidth in parametrically similar ways [40], we explore the dephasing due to an electric field gradient where we have direct control over single-particle broadening by changing the principle quantum number $n$ of the Rydberg state, and thereby the Rydberg polarizability $\alpha_n \propto n^7$. Figure 3(b) shows the loss rate $\gamma_R$ of $|r_c\rangle$ vs $\alpha_n$, obtained by fitting the measured spectra. For spectroscopy of completely independent atoms, $\gamma_R$ would vary in proportion to the inhomogeneous broadening $\gamma_b \propto \alpha_n$ of the Rydberg level. However, the data in Fig. 3(b) vary quadratically with $\alpha_n$. This suppression of decoherence arises because dephasing couples the collective Rydberg state $|r_c\rangle$ to a bath of collective excitations [49] of the hybridized $|r\rangle$ and $|e\rangle$ levels, that, in turn, have no coupling to the cavity mode. In the rotating frame, these states are detuned by $\pm\Omega/2$ relative to the dark polariton [Fig. 3(a)]; for $\gamma_b < \Gamma, \Omega$, this detuning leads to a suppressed loss rate of $s_b\gamma_b^2\Gamma/\Omega^2$ from $|r_c\rangle$; numerical simulations [40] reveal that $s_b \approx 4$, for a normal distribution of Stark shifts with standard deviation $\gamma_b$. The simulations confirm that Doppler decoherence is similarly suppressed, and that while inhomogeneous control-field coupling does

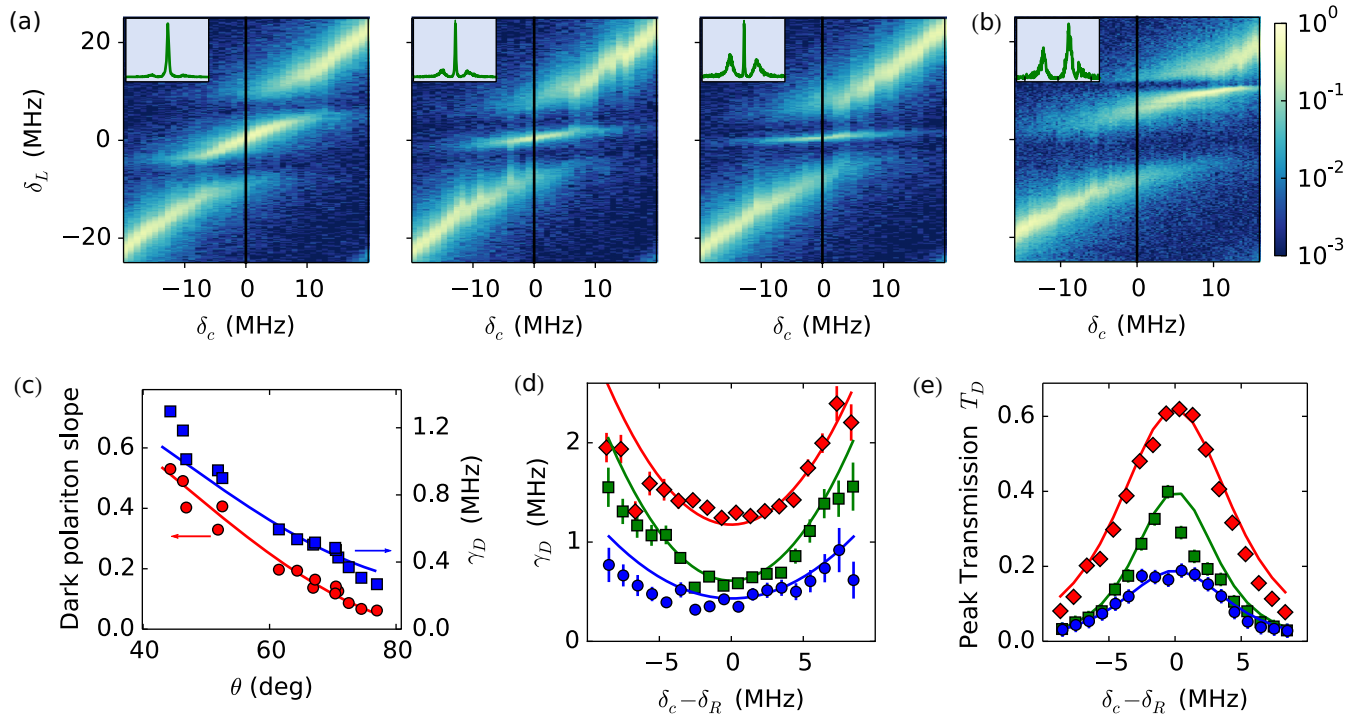


FIG. 2. Spectroscopy of cavity Rydberg polaritons. (a) Cavity transmission spectra as a function of cavity detuning $\delta_c$ for several values of the control laser power. From left to right, $\theta$(deg) = 43, 62, and 72; $\Omega = 13.1(1)$, 6.9(1), and 4.9(1) MHz; $G = 12.3(2)$, 13.0(1), and 14.7(1) MHz. Here, $|\delta_R| < 1$ MHz. Insets in (a) and (b): Spectra along the vertical line at $\delta_c = 0$. Color scale for (a) and (b): Cavity transmission as a fraction of the empty-cavity peak transmission. (b) Transmission spectrum at nonzero control laser detuning $\delta_R = 9.8(4)$ MHz. Here, $\Omega = 8.2(6)$ MHz, $G = 16.8(3)$ MHz. (c) Energy and lifetime vs dark-state rotation angle. Red circles (left): Dark-polariton slope $d\delta_D/d\delta_c$. Blue squares (right): Dark-polariton inverse lifetime $\gamma_D$. Solid lines: Theoretical predictions, using $\Omega$ obtained from the calibrated control laser power and $G$ obtained from fitting to the transmission spectrum. (d) and (e) show the effect of detuning the cavity from EIT resonance using the data in (a). Correspondence to (a): left, diamonds (red); middle, squares (green); right, circles (blue). (d) $\gamma_D$ vs cavity detuning from EIT resonance. Solid lines: Second-order prediction (1), using $\gamma_R$ and $G$ obtained from the transmission spectrum at $\delta_R - \delta_c = 0$. (e) Height $T_D$ of the dark-polariton peak vs cavity detuning. Solid lines: Theoretical prediction using (2) plus higher-order corrections [40] that are only significant for the lower (blue) curve.

renormalize $|r_c\rangle$, a dark state exists [40] which is negligibly broadened by the inhomogeneous coupling.

The suppression of decoherence arising from inhomogeneous broadening does not depend on using Rydberg states, and therefore also applies to ground-state polaritons. In particular, it can be used to improve the coherence time of spin waves in Duan-Lukin-Cirac-Zoller (DLCZ) [23]-style single-photon source experiments [4–6]. Here, we point out that the presence of the control field allows the spin wave to continuously refresh itself, suppressing the decoherence that would otherwise be present; indeed, we predict a parameter regime in which the spin wave lives longer in the presence of the readout field [40].

To employ cavity polaritons in quantum materials, it is essential to harness multiple cavity modes simultaneously. The different cavity modes correspond to the single-polariton spatial eigenstates resulting from motional dynamics in harmonic traps or photonic Landau levels [25,27,36]. For quantum information processing, the different modes can be used to implement one [50] or more [51] qubits. Here, we demonstrate Rydberg EIT in two cavity modes.

Our experimental cavity is designed such that the $TEM_{02}$ and $TEM_{10}$ modes are nearly degenerate, with a separation of $\Delta\delta_c = 20$ MHz, while the $TEM_{00}$ mode is isolated [40]. This mode spectrum allows us to switch seamlessly between single-mode EIT physics in the $TEM_{00}$ mode and multimode physics in the $TEM_{02}$ and $TEM_{10}$ manifold by tuning the cavity length. To demonstrate dark polaritons in two modes, we tune the $TEM_{02}$ and $TEM_{10}$ modes to either side of the atomic resonance. We align the probe beam to couple to both modes, and collect the transmitted light in a multimode fiber. Figure 4(a) shows a measured transmission spectrum for two-mode cavity Rydberg EIT. The two central peaks are dark polaritons in the two modes and are separated by much less than 20 MHz due to strong light-matter mixing. Because the atomic density is approximately uniform across the cavity waist, the cavity modes do not mix, and polaritons form independently in the two modes [40]. The frequencies of the two dark-polariton resonances can then be predicted by considering each mode separately, using the results demonstrated in Fig. 2. In particular, we show in Fig. 4(b) that the splitting $\Delta\delta_D$ between the two dark-polariton peaks tunes with the dark-state rotation angle as $\Delta\delta_D \approx \Delta\delta_c \cos^2\theta$, plus higher-order corrections in $\Delta\delta_c$. The direct relation between the dark-polariton spectrum and the underlying cavity spectrum implies that dark polaritons inherit the dynamics of the cavity modes within the bandwidth $\Gamma_w$, and up to a slowing of time scales by $\cos^2\theta$. Therefore, dark polaritons in multimode

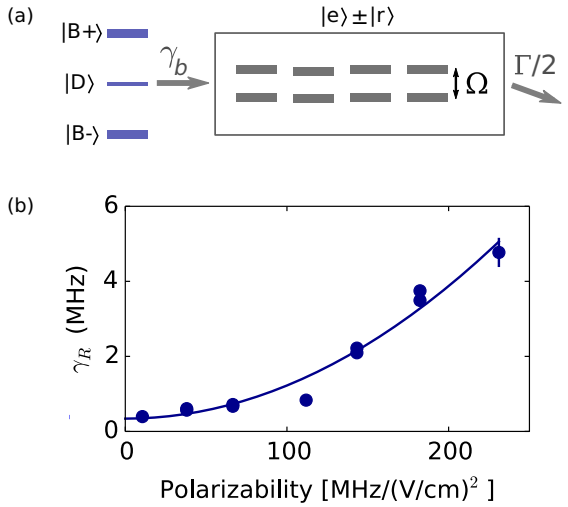


FIG. 3. Collective suppression of decoherence. (a) Inhomogeneous broadening couples the dark polariton to a bath of states orthogonal to the cavity mode. The splitting from the control laser detunes these states from the dark state, suppressing the lossy channel. (b) Effective decay rate $\gamma_R$ of the collective Rydberg state for varying principle quantum number $n$ vs the polarizability of the Rydberg state. Here, $n = 40$, 48, 52, 56, 58, 60, and 62. $\Omega$(MHz) = 7.8(5), $G$(MHz) = 12(2), average and standard deviation (std. dev.) over the data sets. Solid line: Quadratic fit.

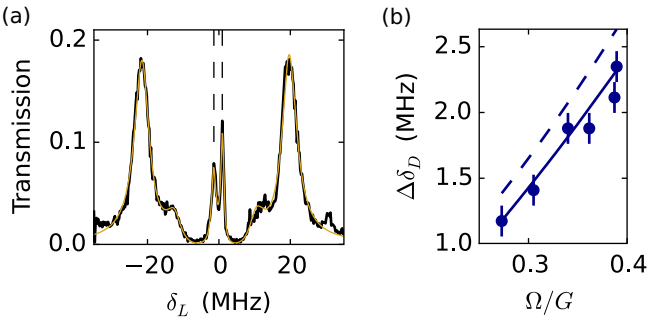


FIG. 4. Rydberg polaritons in two cavity modes. The $TEM_{02}$ and $TEM_{10}$ modes are tuned to ±10 MHz from EIT resonance. (a) Transmission spectrum for $\Omega/G = 0.39$, with $G = 27$ MHz. The dark-polariton resonances (dashed lines) are separated by $\Delta\delta_D = 2.3$ MHz. Curve: Fit to theoretical model for two orthogonal collective states. (b) Adjusting the control laser power varies the photonic component of the dark-polariton states, tuning $\Delta\delta_D$. Dashed curve: First-order prediction. Solid curve: Numerical solution.

cavities inherit the mass, trapping, and effective magnetic field of their photonic constituents [25,27,36].

In conclusion, we have observed Rydberg polaritons in an optical cavity and studied their energy and coherence properties; we demonstrate that the available bandwidth for polariton dynamics and interactions is closely related to the free-space EIT linewidth, and reveal a collective suppression of inhomogeneous decoherence. Introducing polariton-polariton interactions by working with higher Rydberg levels will provide a way to extend single-photon source [12,13] and single-photon transistor [20–22] technology to higher fidelity via an optical cavity. Introduction of near-degenerate multimode cavities [25,27,36] will provide a spatial degree of freedom for exploring exotic condensed-matter models using Rydberg polaritons.

The authors thank Lindsay Bassman, Graham Greve, Aaron Krahn, Sohini Upadhyay, Jin Woo Sung, Michael Cervia, and William Tahoe Schrader for contributions to the experimental system. The U.S. AFOSR (Grant No. FP053419-01-PR) supported apparatus construction and the U.S. DOE (Grant No. FP054241-01-PR) supported theoretical modeling, as well as data collection and analysis.

[1] R. Balili, V. Hartwell, D. Snoke, L. Pfeiffer, and K. West, Science **316**, 1007 (2007).
[2] H. Deng, H. Haug, and Y. Yamamoto, Rev. Mod. Phys. **82**, 1489 (2010).
[3] I. Carusotto and C. Ciuti, Rev. Mod. Phys. **85**, 299 (2013).
[4] C. W. Chou, S. V. Polyakov, A. Kuzmich, and H. J. Kimble, Phys. Rev. Lett. **92**, 213601 (2004).
[5] T. Chanelière, D. N. Matsukevich, S. D. Jenkins, S.-Y. Lan, T. A. B. Kennedy, and A. Kuzmich, Nature (London) **438**, 833 (2005).
[6] J. Simon, H. Tanji, J. K. Thompson, and V. Vuletić, Phys. Rev. Lett. **98**, 183601 (2007).
[7] A. V. Akimov, A. Mukherjee, C. L. Yu, D. E. Chang, A. S. Zibrov, P. R. Hemmer, H. Park, and M. D. Lukin, Nature (London) **450**, 402 (2007).
[8] M. D. Lukin, M. Fleischhauer, R. Cote, L. M. Duan, D. Jaksch, J. I. Cirac, and P. Zoller, Phys. Rev. Lett. **87**, 037901 (2001).
[9] M. D. Lukin, Rev. Mod. Phys. **75**, 457 (2003).
[10] J. D. Pritchard, D. Maxwell, A. Gauguet, K. J. Weatherill, M. P. A. Jones, and C. S. Adams, Phys. Rev. Lett. **105**, 193603 (2010).
[11] A. V. Gorshkov, J. Otterbach, M. Fleischhauer, T. Pohl, and M. D. Lukin, Phys. Rev. Lett. **107**, 133602 (2011).
[12] Y. O. Dudin and A. Kuzmich, Science **336**, 887 (2012).
[13] T. Peyronel, O. Firstenberg, Q. Y. Liang, S. Hofferberth, A. V. Gorshkov, T. Pohl, M. D. Lukin, and V. Vuletić, Nature (London) **488**, 57 (2012).
[14] V. Parigi, E. Bimbard, J. Stanojevic, A. J. Hilliard, F. Nogrette, R. Tualle-Brouri, A. Ourjoumtsev, and P. Grangier, Phys. Rev. Lett. **109**, 233602 (2012).
[15] J. Stanojevic, V. Parigi, E. Bimbard, A. Ourjoumtsev, and P. Grangier, Phys. Rev. A **88**, 053845 (2013).
[16] D. Maxwell, D. J. Szwer, D. Paredes-Barato, H. Busche, J. D. Pritchard, A. Gauguet, K. J. Weatherill, M. P. A. Jones, and C. S. Adams, Phys. Rev. Lett. **110**, 103001 (2013).
[17] C. S. Hofmann, G. Günter, H. Schempp, M. Robert-de-Saint-Vincent, M. Gärttner, J. Evers, S. Whitlock, and M. Weidemüller, Phys. Rev. Lett. **110**, 203601 (2013).
[18] O. Firstenberg, T. Peyronel, Q. Y. Liang, A. V. Gorshkov, M. D. Lukin, and V. Vuletić, Nature (London) **502**, 71 (2013).

[19] P. Bienias, S. Choi, O. Firstenberg, M. F. Maghrebi, M. Gullans, M. D. Lukin, A. V. Gorshkov, and H. P. Büchler, Phys. Rev. A **90**, 053804 (2014).
[20] H. Gorniaczyk, C. Tresp, J. Schmidt, H. Fedder, and S. Hofferberth, Phys. Rev. Lett. **113**, 053601 (2014).
[21] S. Baur, D. Tiarks, G. Rempe, and S. Dürr, Phys. Rev. Lett. **112**, 073901 (2014).
[22] D. Tiarks, S. Baur, K. Schneider, S. Dürr, and G. Rempe, Phys. Rev. Lett. **113**, 053602 (2014).
[23] L.-M. Duan, M. D. Lukin, J. I. Cirac, and P. Zoller, Nature (London) **414**, 413 (2001).
[24] R. Boddeda, I. Usmani, E. Bimbard, A. Grankin, A. Ourjoumtsev, E. Brion, and P. Grangier, arXiv:1512.08480.
[25] A. Sommer and J. Simon, New J. Phys. **18**, 035008 (2016).
[26] J. Klaers, J. Schmitt, F. Vewinger, and M. Weitz, Nature (London) **468**, 545 (2010).
[27] A. Sommer, H. P. Büchler, and J. Simon, arXiv:1506.00341.
[28] D. E. Chang, V. Gritsev, G. Morigi, V. Vuletić, M. D. Lukin, and E. A. Demler, Nat. Phys. **4**, 884 (2008).
[29] S. Gopalakrishnan, B. L. Lev, and P. M. Goldbart, Nat. Phys. **5**, 845 (2009).
[30] J. Otterbach, M. Moos, D. Muth, and M. Fleischhauer, Phys. Rev. Lett. **111**, 113001 (2013).
[31] A. J. Kollár, A. T. Papageorge, K. Baumann, M. A. Armen, and B. L. Lev, New J. Phys. **17**, 043012 (2015).
[32] F. Grusdt and M. Fleischhauer, Phys. Rev. A **87**, 043628 (2013).
[33] M. Hafezi, M. D. Lukin, and J. M. Taylor, New J. Phys. **15**, 063001 (2013).
[34] R. O. Umucalılar, M. Wouters, and I. Carusotto, Phys. Rev. A **89**, 023803 (2014).
[35] M. F. Maghrebi, N. Y. Yao, M. Hafezi, T. Pohl, O. Firstenberg, and A. V. Gorshkov, Phys. Rev. A **91**, 033838 (2015).
[36] N. Schine, A. Ryou, A. Gromov, A. Sommer, and J. Simon, arXiv:1511.07381.
[37] M. D. Lukin, M. Fleischhauer, M. O. Scully, and V. L. Velichansky, Opt. Lett. **23**, 295 (1998).
[38] G. Hernandez, J. Zhang, and Y. Zhu, Phys. Rev. A **76**, 053814 (2007).
[39] M. Fleischhauer, A. Imamoglu, and J. P. Marangos, Rev. Mod. Phys. **77**, 633 (2005).
[40] See Supplemental Material at http://link.aps.org/supplemental/10.1103/PhysRevA.93.041802 for additional details on the experimental implementation, theoretical description, and numerical simulations.
[41] G. Müller, M. Müller, A. Wicht, R.-H. Rinkleff, and K. Danzmann, Phys. Rev. A **56**, 2385 (1997).
[42] H. Wang, D. J. Goorskey, W. H. Burkett, and M. Xiao, Opt. Lett. **25**, 1732 (2000).
[43] H. Wu, J. Gea-Banacloche, and M. Xiao, Phys. Rev. Lett. **100**, 173602 (2008).
[44] M. Mücke, E. Figueroa, J. Bochmann, C. Hahn, K. Murr, S. Ritter, C. J. Villas-Boas, and G. Rempe, Nature (London) **465**, 755 (2010).
[45] T. Kampschulte, W. Alt, S. Manz, M. Martinez-Dorantes, R. Reimann, S. Yoon, D. Meschede, M. Bienert, and G. Morigi, Phys. Rev. A **89**, 033404 (2014).
[46] A. Tauschinsky, R. M. T. Thijssen, S. Whitlock, H. B. van Linden van den Heuvell, and R. J. C. Spreeuw, Phys. Rev. A **81**, 063411 (2010).
[47] H. Hattermann, M. Mack, F. Karlewski, F. Jessen, D. Cano, and J. Fortágh, Phys. Rev. A **86**, 022511 (2012).
[48] S. D. Hogan, J. A. Agner, F. Merkt, T. Thiele, S. Filipp, and A. Wallraff, Phys. Rev. Lett. **108**, 063004 (2012).
[49] J. Honer, R. Löw, H. Weimer, T. Pfau, and H. P. Büchler, Phys. Rev. Lett. **107**, 093601 (2011).
[50] Z.-S. Yuan, Y.-A. Chen, B. Zhao, S. Chen, J. Schmiedmayer, and J.-W. Pan, Nature (London) **454**, 1098 (2008).
[51] A. Grodecka-Grad, E. Zeuthen, and A. S. Sørensen, Phys. Rev. Lett. **109**, 133601 (2012).